J Ther Eng, Vol. 9, No. 3, pp. 580−592, May, 2023

Journal of Thermal Engineering
Web page info: https://jten.yildiz.edu.tr
DOI: 10.18186/thermal.1293033

Journal of Thermal Engineering

Research Article

Second order cyclic analysis of counter flow pulse tube refrigerator

Mahmadrafik CHOUDHARI[1,*], Bajirao GAWALI[1], Prateek MALWE[1], Nandkishor DESHMUKH[1], Rustum DHALAIT[1]

[1]*Department of Mechanical Engineering, Walchand College of Engineering, Sangli, 416415, India*

ARTICLE INFO

Article history
Received: 08 May 2021
Revised: 21 December 2021
Accepted: 25 December 2021

Keywords:
Counter Flow Pulse Tube Refrigerator; Second Order Cyclic Analysis; CFD Modeling

ABSTRACT

Stirling machines are ecologically propitious refrigeration devices that utilize natural gases like helium, nitrogen, or air. Stirling machines are active refrigerators that should be designed with minimal vibrations and durability in order to fulfil current and future commercial demands and requirements. The present paper deals with the modification of the inertance pulse tube refrigerator in which the reservoir is eliminated and replaced with another pulse tube refrigerator. These two pulse tube refrigerators are operated at 180 degrees out of phase, called counter-flow pulse tube refrigerators (CFPTR). The second-order cyclic analysis approach is used to develop a mathematical model for evaluating the performance of CFPTR. This paper describes a modified second-order cyclic approach in detail. The performance of CFPTR is evaluated by estimating the ideal refrigerating effect, ideal power input, and losses individually, yielding net power input and net refrigerating effect. The net refrigerating effect of 30.88W at 70K is obtained with the percentage of Carnot COP of 13.71. The CFD modeling of CFPTR is used to corroborate the second order cyclic model.

Cite this article as: Choudhari M, Gawali B, Malwe P, Deshmukh N, Dhalait R. Second order cyclic analysis of counter flow pulse tube refrigerator. J Ther Eng 2023;9(3):580−592.

INTRODUCTION

The energy-efficient active refrigeration system should be designed with durability and minimal vibrations to fulfil current and future demands. For an energy-efficient system, passive and active heat transfer enhancement techniques are utilized. Two active heat transfer enhancement techniques that have recently been developed include the use of nanofluid in a rotating field and oscillating flow in a refrigeration system [1,2]. Bayareh et al. [3–5] performed a numerical analysis of mixed convection (free and forced convection) heat transfer considering alumina water nanofluid. The analysis involved several configurations, including nanofluid between two cylinders with an inner rotating cylinder, a blade revolving in a square chamber, and an inclined-baffled C type enclosure. The average Nusselt number is affected by dimensionless factors such as Richardson and Rayleigh numbers, nanofluid volume fraction, and eccentricity ratio [3]. In the case of a blade rotating in a square chamber, the effect of blade length is the additional parameter considered. Heat transfer is observed to be proportional to blade length [4]. A numerical study of mixed

***Corresponding author.**
*E-mail address: mahmadrafik.choudhari@walchandsangli.ac.in

This paper was recommended for publication in revised form by Regional Editor Ahmet Selim Dalkılıç

Published by Yıldız Technical University Press, İstanbul, Turkey
Copyright 2021, Yıldız Technical University. This is an open access article under the CC BY-NC license (http://creativecommons.org/licenses/by-nc/4.0/).

convection heat transfer in inclined-baffled C-type enclosures stated that heat transfer increases with an increase in enclosure angle and length of the baffle [5]. Oscillating flow heat transfer is an active heat transfer enhancement technique used in pulse tube refrigeration systems to eliminate heat quickly and efficiently. Pulse Tube Refrigerator (PTR), first discovered by Gifford and Longsworth [6], has the potential to be widely applied for producing low temperatures. The main benefit of this system is the absence of moving mechanical parts in low-temperature regions. It lowers the induced mechanical vibrations significantly and enormously improves the reliability of the subsystems. Based on phase shift, the main two design variations are proposed, and they are the orifice pulse tube refrigerator (OPTR) [7], double inlet OPTR [8], and the inertance pulse tube refrigerator (IPTR) [9]. According to speed and valve arrangement, PTR is classified as Stirling type and G-M type PTR. The G-M pulse tube is consists of a rotary valve and has low-frequency flow, while the Stirling type pulse tube has no valve mechanism and operates with high frequency. The thermodynamic cycle of the Stirling refrigerator and Stirling type PTR is more or less similar to each other and can be seen as a replacement of the displacer by a gas piston. A passive phase shifter replaces the active phase shifter. In the PTR system, refrigerating effect is obtained by maintaining the appropriate phase shift between the mass flow and pressure pulse at the cold end of the pulse tube [10,11]. Pulse tube refrigeration is defined as continuous pressurization and depressurization with air or gas as the working medium, creating a temperature gradient in the pulse tube. The inertance type of the pulse tube refrigerator is presented in Figure 1 [12]. The current work is concerned with the analysis of modified PTR.

The reservoir occupied a substantial fraction of pulse-tube refrigerator volume. The reservoir volume is ten times more than the pulse tube volume, which affects on specific power of the PTR, and it is not favorable for small size, lightweight PTR. So reservoir is removed and replaced by another set of PTR. Two sets of PTR are connected by an inertance tube at hot end heat exchangers, as shown in Figure 2. Volume flow at CHX has adjusted so that total volume flow at inertance tube junction is zero, allowing the

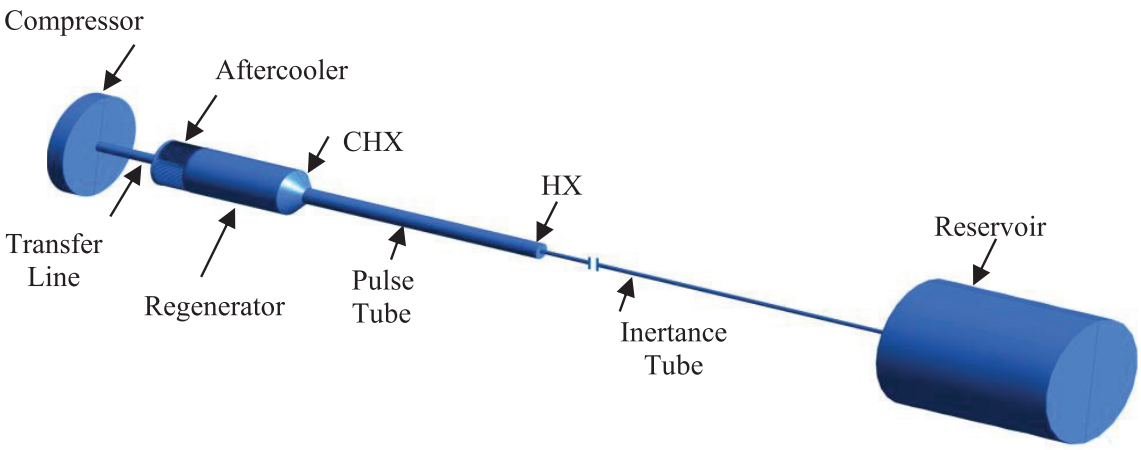

Figure 1. Inertance pulse tube refrigerator system.

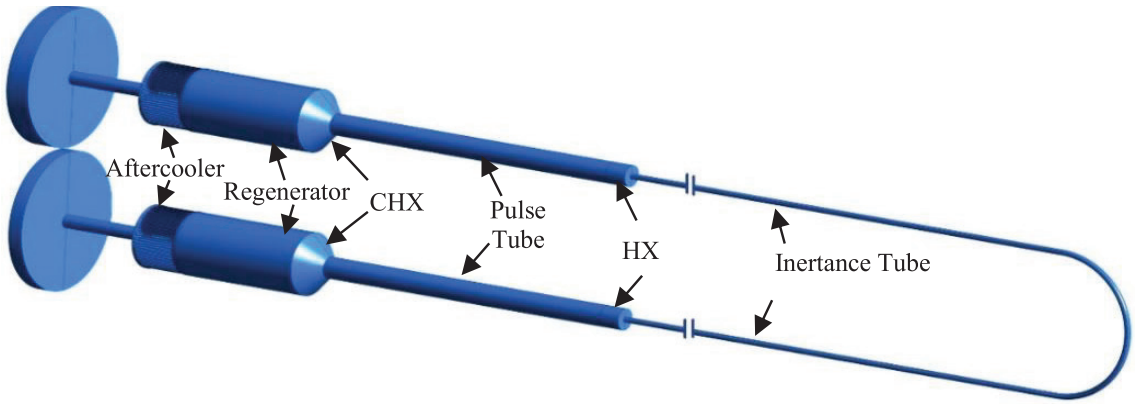

Figure 2. Counterflow pulse tube refrigerator system

reservoir removal [13,14]. Initially, Gao et al. [15] came up with a new concept of phase shift controller (on-off valve at pulse tube hot ends) by eliminating reservoir to increase refrigeration efficiency. Zhang et al. [16] studied the inert phasing pulse tube refrigerator numerically. The result of the study revealed that it performs better than the orifice type of pulse tube refrigerator. Gour et al. [17] designed twin PTR using Sage 6.0. The simulation result shows that COP of twin PTR is doubled as compared to single PTR.

The proposed system is the modification of the Gawali et al. [18] model, which comprises two Stirling type PTR. The two identical pulse tubes are connected by an inertance tube at HHX, eliminating the reservoir of IPTR. This system is Stirling-type Counter Flow Pulse Tube Refrigerator (CFPTR) system displayed in Figure 2. The two identical compressors operating in a 180-degree phase shift develop the pressure waves. A special feature of the proposed system is that the pressure wave is generated by two identical compressors operating 180 degrees out of phase in such a way that one tube is high-pressure side and another tube is low-pressure side. After every 180 degrees of crank angle, the flow gets reversed in direction.

There are many models, which simulate the PTR. However, due to simplicity, the isothermal model is still extensively used. The isothermal model can provide comprehensive clarity by considering the actual process occurring in the system to some level. Zhu and Chen [19] presented the isothermal model for OPTR. They compared the ideal performance, did not consider the losses, and assumed an isothermal compression process. The analysis of Zhu et al. [19] was modified by Atrey and Narayankhedkar [20] by including the losses and thus making it a second-order analysis. Both Zhu et al. [19] and Atrey et al. [20] considered orifice as a phase shifter, and the compression process isothermal. Zhu et al. [21,22] extended the cyclic analysis approach to the modified pulse tube refrigerator.

In practice, the process of compression is neither isothermal nor adiabatic. However, due to high speed (40 to 50 cycles/sec), the compression process tends to be close to the adiabatic process. Hence, the assumption of adiabatic compression is more realistic for a high-frequency PTR system. Narayankhedkar et al. [23] developed a model for the adiabatic compression process. With the adiabatic compression process, there is a need to use an after-cooler which reduces the discharge temperature. Shendage et al. [24,25] performed cyclic analysis and optimization of the Stirling engine by developing the adiabatic model. Natu et al. [26] applied the cyclic approach and presented the performance evaluation of a two-stage Stirling cryogenerator.

The present paper develops the second-order adiabatic model to analyze CFPTR by the cyclic analysis approach. A modified analysis approach is presented to determine ideal power input, ideal refrigerating effect, and losses separately, providing estimates of net power input and net refrigerating effect. Then confirmation of the present model is done by CFD modeling of CFPTR.

Cyclic analysis

The second-order adiabatic model is developed to analyze the CFPTR. The ideal cycle processes differ from the actual cycle processes due to the losses, resulting in an increment in net power supply and a decrement in net refrigeration effect. Several expressions are available in the literature to obtain pressure drops in the regenerator. Also, there are various relationships available for the estimation of various losses because of which the available refrigeration effect decreases. So, the following assumptions are made during the cyclic analysis of CFPTR.

1. Pulse tube gas splits into three parts, I, II, and III, shown in Figure 3. Part I is gas at HHX. Part II is the middle part, similar to the displacer, and part III is gas at CHX.
2. The pressure remains the same at any instant in the system.
3. The regenerator dead space temperature is the logarithmic mean temperature of cold end and hot end regenerator temperatures.
4. There is no direct thermal diffusion between adjacent gas elements in the pulse tube.
5. There is the sinusoidal movement of the piston.
6. The piston seal is gas leak-proof.
7. There is no resistance to the fluid.
8. The working fluid is considered an ideal gas.
9. The dependency of material properties on temperature.

A pressure-volume cycle of 360^0 is divided into 72 small intervals to carry out the cyclic analysis. The ideal gas law is applied for each interval, and the equation is rearranged to give the pressure for the corresponding point of the interval. Mass flow rates, the ideal refrigerating effect, and ideal power input are calculated based on the volume variations in the I, II, and III sections. There are various losses because of which the available refrigeration effect decreases. After considering these losses, the net refrigerating effect, net power input, and COP is calculated.

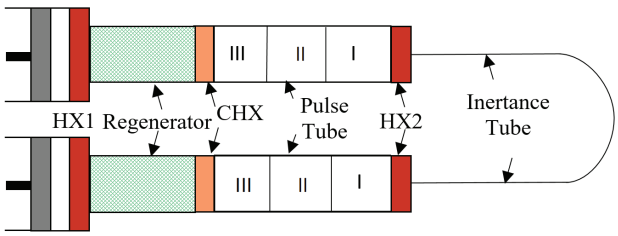

Figure 3. CFPTR system with pulse tube sections

Pressure volume variation

Two identical pulse tube refrigerators are connected through an inertance tube at the hot end exchanger, operating at 180 degrees out of phase shift.

The volume variation in the compression space is sinusoidal, and it is given as

$$V_{c1} = V_{cd1} + V_{cm1}\left(1 + cos\right)/2 \quad (1)$$

$$V_{c2} = V_{cd2} + V_{cm2}\left(1 + cos\ \alpha\right)/2 \quad (2)$$

Where $\alpha = (180 - \theta)$, V_{cd} is the clearance volume. The total mass of the working fluid is

$$M = M_c + M_{h1} + M_r + M_{h2} + M_e \quad (3)$$

P is the pressure developed in each time interval of the cycle, and it varies with crank angle. Using the perfect gas laws

$$P = \frac{MR}{\frac{V_c}{T_c} + \frac{V_{h1}}{T_c} + \frac{V_r}{T_r} + \frac{V_{h2}}{T_e} + \frac{V_e}{T_e}} \quad (4)$$

The product MR of total mass moles of the gas, M, and universal gas constant, R, is assumed to be unity for initial iteration, as the exact value of M is not known. The new MR value is obtained after the simulation of one complete cycle. The complete cycle is split into 72 equal intervals of 5^0 crank-angle. The pressure in the CFPTR system for each interval is then obtained as

$$P(1) = \frac{1}{\frac{V_c(1)}{T_c(1)} + \frac{V_{h1}}{T_c} + \frac{V_r}{T_r} + \frac{V_{h2}}{T_e} + \frac{V_e(1)}{T_e(1)}} \quad (5)$$

$P(1)$ indicates the pressure developed in the working space during the first interval of the cycle. $Vc(1)$ and $Ve(1)$ during the first interval of the cycle, respectively. Tc (1) is the gas temperature in the compression space for the first interval.

Assuming

$$T_c(2) = T_c(1)\left[\frac{P(2)}{P(1)}\right]^y \qquad y = (\gamma - 1)/\gamma \quad (6)$$

Where T_c (2) and P(2) are the gas temperature in the compression space and gas pressure in the working space for the second interval of the cycle, respectively. Substitute the values of Vc(2), $T_c(2)$ and $Ve(2)$ in equation (5), $P(2)$ is the only unknown variable in the equation, and it is calculated by the Newton-Raphson method. $P(3)$ is calculated by using $P(2)$ and so on. If q is equal to 5^0, values of pressures and temperatures up to the 73rd interval need to be calculated to come to the starting position. The pressure and temperature values should be the same at the 1st and 73rd intervals to show it is a cyclic process.

The expansion space volume is assumed as 1% of the volume variation in compression space.

$$V_e = 0.01V_c \quad (7)$$

As all the points are equispaced on the P-q curve, and the curve is symmetrical, the mean pressure P_m would be equal to

$$P_m = \frac{P_{total}}{72} \quad (8)$$

Where P_{total} is the summation of pressure values in all 72 intervals, i.e., in one cycle. The existing average pressure P_{avg} of the CFPTR system is known. The ratio of P_{avg} to P_m obtains the correct value of product MR. Initially, MR is supposed to be 1. So, with the new MR values, the corrected pressure for each interval is calculated by multiplying the same with MR.

The calculation of pressure and volume variation is completed with assumed volume variation in expansion space Ve. Correction in the expansion space volume variation depends on the phase shifter (inertance) mechanisms. Using the characteristic equation of the phase shifter, the volume variation in the expansion space is possible and it is made by calculating mass flow through section I (m_I). Then the volume of pulse tube section I is calculated using m_I. Volume variation in pulse tube section III is calculated using V_I, V_{II} and pulse tube volume V_{pt}.

The mass flow rate through the inertance will depend on the pressure in the pulse tube set I and pulse tube set II. If the pressure in the pulse tube of the first set (P_1) is greater than the pulse tube of the second set (P_2), gas will flow from PTR set I to PTR set II and vice versa.

For inertance tube, the characteristic equations are:

For $P_1 > P_2$

$$m_0 = 0.25 \times \pi \times itd^2 \left[\frac{(P_1 - P_2) \times itd}{itl \times f \times V_{h3}}\right]^{0.5} \quad (9)$$

For $P_1 < P_2$

$$m_0 = -0.25 \times \pi \times itd^2 \left[\frac{(P_2 - P_1) \times itd}{itl \times f \times V_{h3}}\right]^{0.5} \quad (10)$$

Mass flow rate at section I

The mass flow from section one depends upon the mass flow through inertance (m_o) and the pressure variation in volume I

$$m_I = m_o + \frac{V_{h3}}{RT_c}\left[\left(P_{i+1} - P_{i-1}\right)\times\left(0.5\times n\times n_{max}\right)\right] \quad (11)$$

Calculating the volumes VI, VII, and VIII

The hot end isothermal volume V_I is calculated as

$$V_I = \frac{m_I \times R \times T_c}{P} \quad (12)$$

The adiabatic part of the pulse tube V_{II}

$$V_{II} = C\left[P\right]^{1/\gamma} \quad (13)$$

The correct value of C is obtained with

$$V_{III\,min} = 0.0 \quad (14)$$

The expansion space volume or cold end side of pulse tube volume V_{III} is obtained as

$$V_{III} = V_{pt} - \left(V_I + V_{II}\right) \quad (15)$$

Ideal power input and ideal refrigerating effect

Pressure and volume variation calculation is done for the cycle and the same is used for computation of the ideal power input (Q_P), and the ideal refrigeration effect (Q_R).

$$\begin{aligned} Q_P(I) &= \int P(I)\,dV_I(I) \\ Q_R(I) &= \int P(I)\,dV_e(I) \end{aligned} \quad (16)$$

Loss analysis

Loss analysis of the CFPTR takes account of the actual processes in the system that degrades the system's performance. Due to the losses, compressor power input increases, and the refrigerating effect get decreases. The friction factor 'f' and pressure drop DP are calculated with the correlations used by Martini [27] for different mass flow rates at different intervals.

$$\Delta P = \frac{f\,L\,G^2}{2\rho r_h} \quad (17)$$

Where f is calculated as

$$\log f = 1.73 - 0.93\log Re \qquad Re < 60 \quad (18)$$

$$\log f = 0.714 - 0.365\log Re \qquad 60 < Re < 1000 \quad (19)$$

$$\log f = 0.015 - 0.125\log Re \qquad Re > 1000 \quad (20)$$

Where Re is the Reynolds number given by the formula

$$Re = \frac{G\times itd}{\mu} \quad (21)$$

Regenerator ineffectiveness loss

The regenerator is the major source of loss. Because of the regenerator's ineffectiveness, the gas is cooled to (T_e + DT) instead of T_e. Therefore some refrigeration effect is lost to cool the gas coming out from the regenerator. The loss, Q_{REG}(I), for the Ith interval is given by, as described by Martini [27]

$$Q_{REG}(I) = (W_{RS}(I)\times C_V\times(T_c - T_e))\tau\times\frac{2}{NTU+2} \quad (22)$$

Loss due to temperature swing

Temperature swing loss occurs due to the change in matrix temperature. The change in regenerator matrix temperature, as given by Martini [27], is

$$D_{RMT}(I) = \left[\frac{W_{RS}(I)\times C_V\times(T_c - T_e)}{N_U\times M_{MX}\times C_{PM}}\right] \quad (23)$$

D_{RMT}(I) starts at zero at the start of flow and grows to D_{RMT}(I) at the end of the flow during the interval. The loss is given by

$$Q_{TS}(I) = 0.5\times W_{RS}(I)\,C_V\,D_{RMT}(I)\times\tau \quad (24)$$

P-V loss due to pressure drop

The expansion space pressure values are calculated as per the given equation P_e(I) = P(I) - (pressure drop at the interval). Due to pressure drop, there is a reduction in the refrigeration effect. So, the actual refrigeration effect is given as

$$Q_{IP}(I) = \int P_e(I)\,dV_e(I) \quad (25)$$

The term $Q_R - Q_{IP}$ gives the P-V loss.

Conduction loss through solid members

The losses due to conduction are calculated as,

$$Q_K = k_{mx}\,A_k\left(T_c - T_e\right)/L \quad (26)$$

Martini [27] has given a formula for effective thermal conductivity, $k_{mx.}$ Factor FF is the (1 – porosity) for the mesh used in the matrix.

$$k_{mx} = k_g\,\frac{\dfrac{1+k_m/k_g}{1-k_m/k_g} - FF}{\dfrac{1+k_m/k_g}{1-k_m/k_g} - FF} \quad (27)$$

Computer code

The above governing equations are converted into computer code using C programming. Figure 4 shows a flow chart for the same.

Results of the cyclic model

The major geometrical and operating conditions of CFPTR considered for analysis are given in Table 1. The pressure, volume, and mass flow variation through the

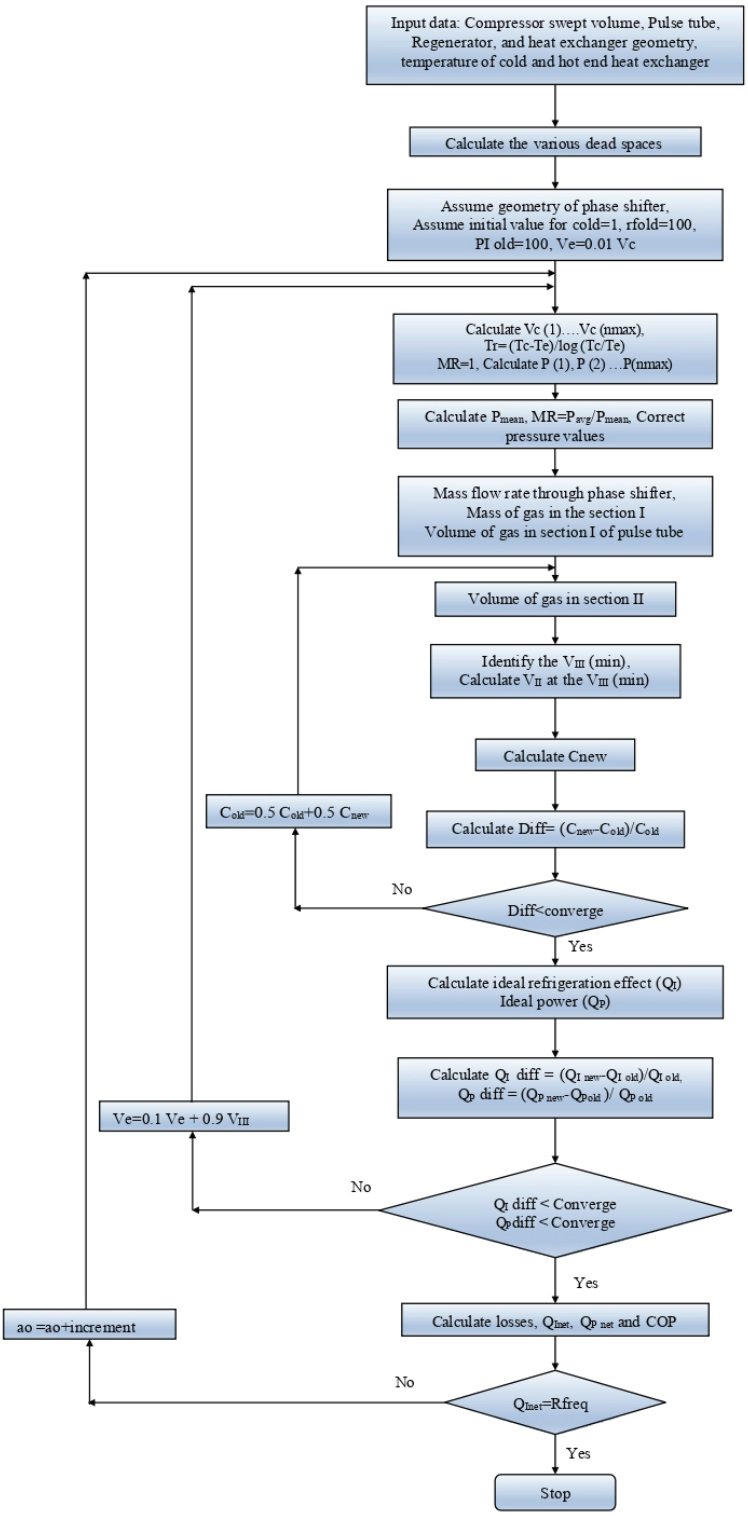

Figure 4. Flow chart.

inertance tube is computed and plotted to calculate the ideal power input and ideal refrigerating effect. Then losses calculation provides an estimation of net power input and net refrigerating effect.

Table 1. Major geometrical and operational parameters of CFPTR

Component / parameter	Unit	Values
Pulse tube diameter	mm	9.6
Compressor swept volume	cm^3	30
Volume of pulse tube	cm^3	9.3
Operating frequency	Hz	50
After cooler volume	cm^3	5.3
Regenerator OD	mm	28
Regenerator length	mm	54
Regenerator mesh	Mesh / in.	400
Cold end heat exchanger volume	cm^3	1.8
Hot end heat exchanger volume	cm^3	0.45
Average pressure	bar	16
Heat rejection temperature	K	310
Refrigeration temperature	K	70

The pressure variation in the two subsystems of CFPTR is obtained, and they are in a 180-degree phase shift. The compression space pressure variation of PTR set I and PTR set II over a cycle with crank angle is presented in Figure 5. The maximum and minimum pressure in the system is 18.12 bar and 14.08 bar, respectively. Pressure variation for the cycle is useful to find the ideal power input and refrigerating effects.

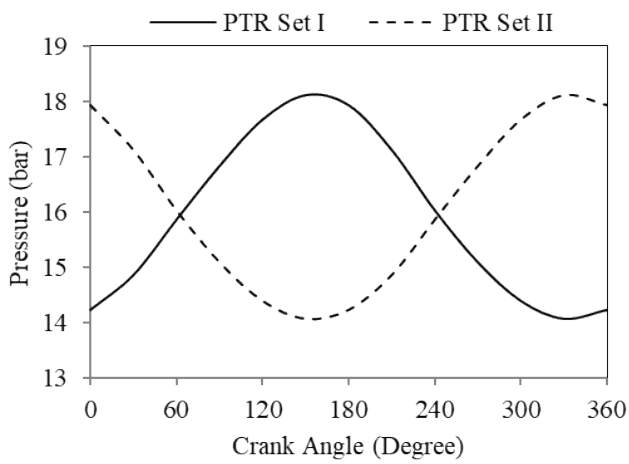

Figure 5. Compressor pressure vs crank angle.

Volume variation

The compression volume variation in PTR set I and PTR set II over a cycle with crank angle is displayed in Figure 6. The maximum and minimum volume in the system is $3.03X10^{-5}$ m^3 and 3.00 $X10^{-7}$ m^3, respectively.

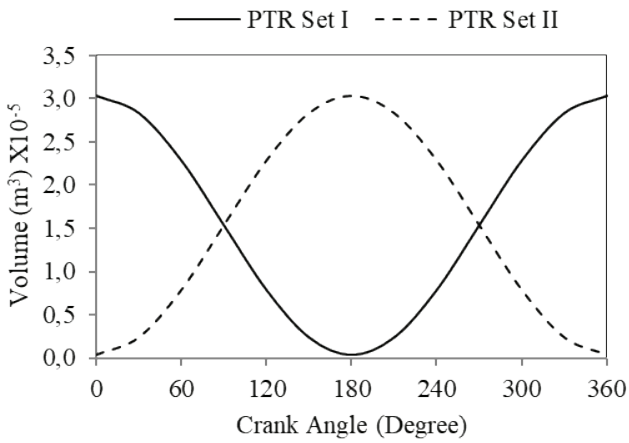

Figure 6. Compressor volume vs crank angle

Mass flow rate through the inertance tube

The mass flow rate through the inertance tube for PTR set I is calculated using equations (9) and (10) and shown in Figure 7. It depends on the pressure in the pulse tube and pressure in the PTR set II. If the PTR set I pressure exceeds PTR set II, gas will flow from the set I to set II.

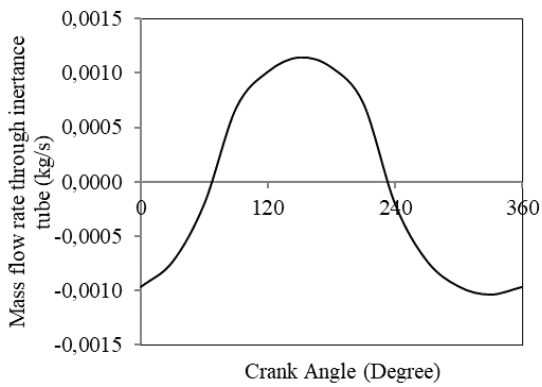

Figure 7. Mass flow rate through the inertance tube for PTR Set I vs crank angle.

The compression and expansion pressure-volume variation is shown in Figure 8. The area under the PV curve gives the ideal work of the compressor and refrigerating effect for a cycle.

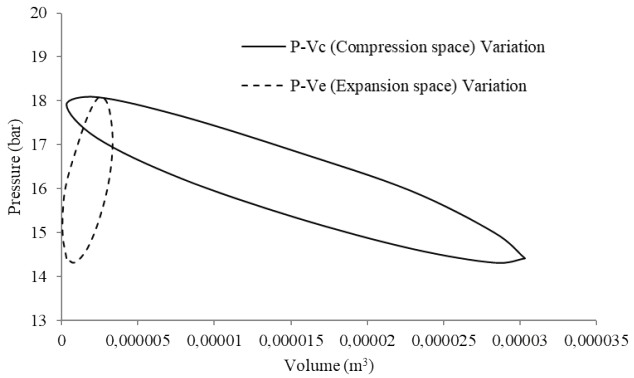

Figure 8. P-V charts for compression and expansion space.

The ideal power input, Q_P, and the ideal refrigeration effect, Q_R, to the system are calculated using pressure-volume variation for the cycle. The values of the net refrigerating effect and losses for CFPTR are displayed in the form of a pie chart in Figure 9. The ideal and net power input to the compressor of CFPTR, COP, Carnot COP, and percentage of Carnot COP calculation has been made, and they are displayed in Table 2.

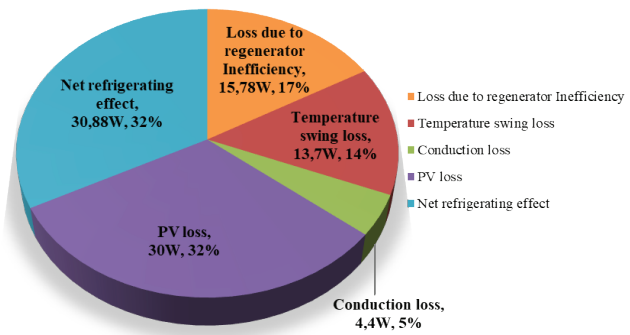

Figure 9. Net refrigerating effect and losses.

Table 2. Performance parameters of CFPTR

Parameter	Unit	Value
Gross Refrigerating effect	W	94.76
Net Refrigerating effect	W	30.88
Compressor power (Ideal)	W	438
Regenerator pressure drop	W	95.34
Heat exchanger pressure drop	W	58.6
PV power	W	591.94
Net power input (78 % motor efficiency)	W	758.89
COP		0.04
Carnot COP		0.29
Percentage of Carnot COP		13.7

The performance evaluation of CFPTR is done by using a cyclic analysis approach. The net refrigerating effect and net power input are given for the CFPTR system. To validate, the CFD model is prepared using geometrical parameters, and the load of 15 W at each CHX is provided to obtain cyclic steady temperature.

CFD Analysis of CFPTR

CFD software is widely used for numerical simulation-based systems studies, such as fluid flow, heat transfer, and chemical reaction phenomena. The CFD analysis requires geometry creation, meshing, and solver setup with appropriate boundary conditions. The governing equations are solved for velocity, pressure, and temperature at various locations in the system. CFD may also be used to model regenerators and heat exchangers that use porous material. Designers may need to create a unique profile as a boundary condition in some cases, and these conditions cannot be expressed using FLUENT's default settings. For defining such conditions, FLUENT introduces the UDF option. CFD allows for compressor modeling using dynamic meshing and appropriate UDF.

CFD analysis of CFPTR is performed to corroborate the results obtained by cyclic analysis. It is conducted to predict the cycle steady temperature at the CHX under no-load and 15 W load conditions. It is to be compared with the cyclic analysis CHX temperature for validation. ANSYS Fluent 18.0 software package is used for CFD simulation with a computer specification of 2.40 GHz processor and 4.00 GB RAM. It takes a month or more to complete a simulation. The working fluid for CFPTR is helium, while the component materials are copper and steel.

Simulated system

The IPTR may be modeled as plane-symmetric around the common plane of the system since the components are cylindrical and conical. Geometry is created using the design modeler in the ANSYS workbench. Table 3 lists the dimensions of the CFPTR model. The "Add Frozen"

Table 3. CFPTR dimensions

Component	Radius (cm)	Length (cm)	Volume(cm³)
Compressor	3.09	1.3	30
Transfer line	0.3	3.796	5.3
Aftercooler	1.4	2.0	
Regenerator	1.4	5.4	22.35
CHX	1.4	0.879	1.8
Pulse tube	0.48	12.85	9.3
HHX	0.50	0.9	0.45
Inertance tube	0.125	200	9.8175

technique is utilized instead of "Add Material" to prevent system components from blending together. The CFPTR geometry view is shown in Figure 10.

The model is meshed with hexahedral elements, with some triangular elements in ANSYS workbench meshing. The mesh must match the interfaces of the various components. A mesh independence test is conducted to obtain optimum meshing for the model. The meshing view and mesh independence test are depicted in Figure 11 and Figure 12, respectively.

The governing equations used in the simulation for the gas domain are given by

Figure 10. CFPTR model.

Figure 11. Mesh view.

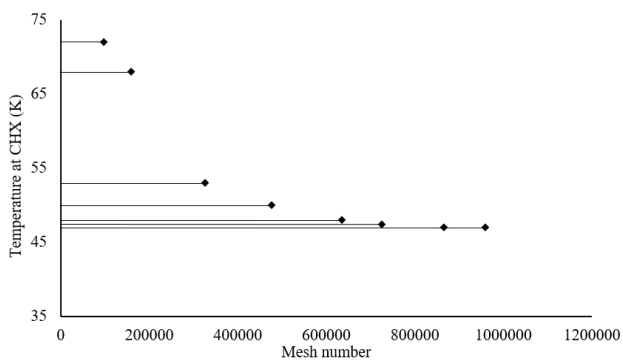

Figure 12. Mesh independency test.

Mass:

$$\frac{\partial \rho}{\partial t}+\nabla\cdot\left(\rho\vec{u}\right)=0 \tag{28}$$

Momentum:

$$\frac{\partial}{\partial t}\left(\rho\vec{u}\right)+\nabla\cdot\left(\rho\vec{u}\vec{u}\right)=-\nabla p+\nabla\cdot\left(\bar{\bar{\tau}}\right) \tag{29}$$

Energy:

$$\frac{\partial}{\partial t}\left(\rho E\right)+\nabla\cdot\left(\vec{u}\left(\rho E+p\right)\right)=\nabla\cdot\left(k_{eff}\nabla T+\left(\bar{\bar{\tau}}_{eff}\cdot\vec{u}\right)\right) \tag{30}$$

Where $\vec{u}$ is the fluid velocity. Similarly, the governing equation used in the simulation for the porous zones are given as

Mass:

$$\frac{\partial\left(\varepsilon\rho\right)}{\partial t}+\nabla\cdot\left(\varepsilon\rho\vec{u}\right)=0 \tag{31}$$

Momentum:

$$\frac{\partial}{\partial t}\left(\varepsilon\rho\vec{u}\right)+\nabla\cdot\left(\varepsilon\rho\vec{u}\vec{u}\right)=-\varepsilon\nabla p+\nabla\cdot\left(\varepsilon\bar{\bar{\tau}}\right)+S_i \tag{32}$$

Where S_i is the source term and it is the combination of the Darcy term and the Forchheimer term [28]:

$$S_i=-\left(\frac{\mu}{\alpha}u+C_2\frac{1}{2}\rho u_{mag}u\right) \tag{33}$$

Where C_2 is the inertial resistance factor and α is the permeability.

$$\alpha=\frac{D_p^{\,2}}{\left(1-\varepsilon\right)^2}\frac{\varepsilon^3}{150} \tag{34}$$

$$C_2=\frac{\left(1-\varepsilon\right)}{D_p}\frac{3.5}{\varepsilon^3} \tag{35}$$

Energy:

$$\frac{\partial}{\partial t}\left(\varepsilon\rho_f E_f+\left(1-\varepsilon\right)\rho_s E_s\right)+\nabla\cdot\left(u\left(\rho_f E_f+p\right)\right)=\nabla\left(k_{eff}\nabla T+\left(\bar{\bar{\tau}}_{eff}\,u\right)\right) \tag{36}$$

Where, E_f = Fluid energy
E_s = Solid medium energy

The cell zone and boundary conditions are applied to the CFPTR system. UDF has been written for the movement of the piston in the compressor [29]. Adiabatic wall condition is given for compressor, regenerator, pulse tube,

and inertance tube while heat exchanger walls have been given as isothermal condition. For hot end heat exchangers, 310 K is given. The material for heat exchangers is specified as copper, and they are considered as porous zone, while the remaining components are made of stainless steel. Patching has been done to reduce computation time for 15 W load conditions by writing linear algebraic equations no. 33 and 34 for regenerator and pulse tube temperature [28,30].

$$T_r = (X - 0.0568)(-4444.44) + 310 \tag{37}$$

$$T_{pt} = (X - 0.1195)(1867.70) + 70 \tag{38}$$

Results of CFD model

The simulation of CFPTR is done to confirm the results obtained by cyclic analysis. The simulation is carried out until the cyclic steady temperature is achieved. In order to have a better understating of temperature variation in CFPTR, the contour is plotted in Figure 13. The temperature contour does not cover the inertance tube. The CFPTR operates in the opposite phase. The pressurization occurs in the pulse tube refrigerator set I, while depressurization occurs in another. So temperature variation in compressor due to the same is displayed in the form of temperature

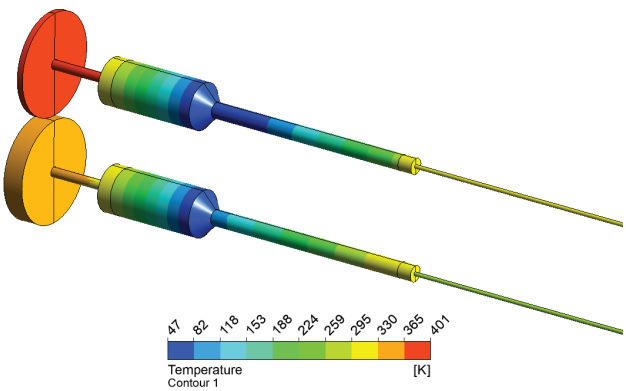

Figure 13. Temperature contour.

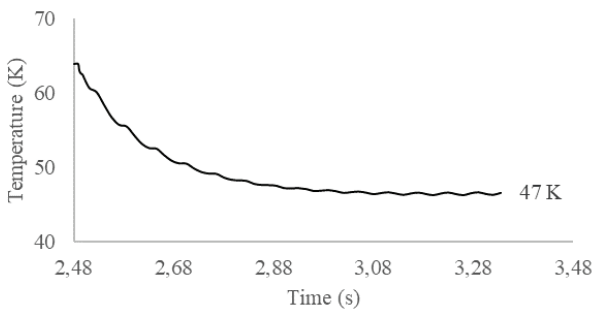

Figure 14. Cooldown curve at 15W load condition.

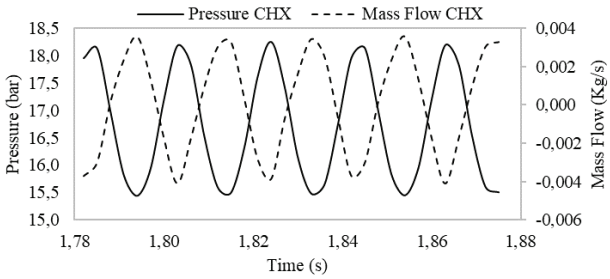

Figure 15. Pressure and mass flow rate at CHX

contour. Figure 14 shows the temperature at CHX with respect to flow time at 15 W load. The phase difference between mass flow and pressure pulse at CHX is useful, and it is crucial for the system's performance, which is plotted in Figure 15.

To reduce computation time, ANSYS Fluent gives a patching tool where the initial value can be patched. For regenerator and pulse tube, temperatures at the cold and hot end are maintained at 70 K and 310 K. Patching for the regenerator and pulse tube is done by equation no. 33 and 34. The cyclic steady temperature of 47 K is attained at CHX for the 15 W load condition. In CFD analysis of CFPTR, the gas domain is taken into account without consideration of wall thickness. Axial conduction losses are significant as a large temperature gradient along the regenerator and pulse tube length. Therefore the wall thickness of tubes should be designed to sustain pressure and reduce axial conduction loss. As a result, conduction losses in solid-state components such as the regenerator and pulse tube are not reflected in the result.

The regenerator is modeled as a porous zone in CFD analysis of CFPTR. The thermal equilibrium model or the thermal non-equilibrium model can be employed to investigate regenerators. In the thermal equilibrium model, the temperature of the gas and wire mesh is supposed to be the same at all times. The thermal equilibrium model is utilized to avoid the problem's complexity.

CONCLUDING REMARKS

The CFPTR system is the modified IPTR obtained by removing the reservoir and replacing it with another pulse tube refrigerator. The current work is about the performance evaluation of the CFPTR system. A mathematical model is developed for the analysis based on the second-order cyclic analysis approach. This paper described a modified second-order cyclic approach for the CFPTR system in detail. The CFPTR performance is assessed by evaluating the ideal refrigerating effect, power input, and losses separately, yielding net power input and net refrigerating effect. The net refrigerating effect and net power input obtained from the analysis of the CFPTR system are 30.88 W and 758.89 W at 70K. The COP and percentage of Carnot COP

obtained for the CFPTR system are 0.04 and 13.71%. The confirmation of the second-order cyclic analysis model is made by CFD analysis by obtaining cyclic steady-state temperature at CHX. This analysis gives the design methodology for the modified system. The experimental setup will be developed for the CFPTR system, and it will be examined in a subsequent paper.

NOMENCLATURE

A_k	Area for heat conduction, m^2
C	Constant
COP	Coefficient of performance
C_{PM}	Specific heat of regenerator matrix, J/kg.K
C_v	Specific heat at constant volume for the gas, J/kg.K
D_p	Wire diameter, m
D_{RMT}	Temperature change for regenerator material, K
E	Total energy of the fluid
f	Friction factor
G	Mass velocity, kg/m^2s
h	Coefficient of heat transfer, $W/m^2 K$
itd	Diameter of inertance tube, m
itl	Length of inertance tube, m
I	Interval
k_g	Gas thermal conductivity, W/m K
k_{mx}	Matrix material thermal conductivity, W/m K
k_{eff}	Effective thermal conductivity, W/m K
M	Total moles of gas in working space, kg-mole
M_c	Moles of gas in compression space, kg-mole
M_{h1}	Moles of gas in aftercooler (dead space), kg-mole
M_r	Moles of gas in regenerator, kg-mole
M_e	Moles of gas in expansion space, kg-mole
M_{h2}	Moles of gas in cold end heat exchanger (dead space), kg-mole
m_I	Mass flow at pulse tube section I, kg/s
m_o	Mass flow through inertance, kg/s
M_{MX}	Mass of matrix material, kg
n_{max}	Number of intervals
NTU	Number of transfer unit
N_U	Nusselt number
P	Pressure, bar
P[i]	Pressure in CFPTR at the distinct interval, bar
P_{avg}	Average pressure, bar
P_m	Mean pressure, bar
Q_{IP}	Refrigerating effect lost due to pressure drop, W
Q_K	Loss due to conduction, W
Q_P	Ideal power input, W
Q_R	Ideal refrigeration effect, W
Q_{REG}	Heat loss due to regenerator ineffectiveness, W
Q_{TS}	Temperature swing loss, W
r_h	Hydraulic radius
R	Universal gas constant, J/kg-mole·K
Re	Instantaneous Reynolds number
T_r	Regenerator Temperature, K
T_e	Temperature in expansion space, K
T_{pt}	Pulse tube temperature K
t	Time, s
V	Volume, m^3
V_{h1}	Aftercooler volume, m^3
V_{h2}	Cold end heat exchanger (CHX) volume, m^3
V_{h3}	Hot end heat exchanger (HHX) volume, m^3
V_{pt}	Pulse tube volume, m^3
W_{RS}	Mass flow rate of helium in the regenerator, kg/s

Greek Symbol

g	Specific heat ratio
q	Crank angle for compressor 1, degree
r	Density, kg/m^3
α	Crank angle for compressor 2, degree
ε	Porosity
t	Time interval
μ	Dynamic viscosity

Subscripts

c	Compression space
cd	Clearance space
cm	Compressor swept volume
e	Expansion space
I	Part I of pulse tube
II	Part II of pulse tube
III	Part III of pulse tube
m	Mean
min	Minimum
pt	Pulse tube
pv	PV work

Abbreviations

CHX	Cold end heat exchanger
CFD	Computational fluid dynamics
CFPTR	Counterflow pulse tube refrigerator
COP	Coefficient of performance
CPU	Central processing unit
HX	Hot end heat exchanger
IPTR	Inertance tube pulse tube refrigerator
OPTR	Orifice pulse tube refrigerator
PTR	Pulse tube refrigerator
RAM	Random access memory
UDF	User defined function

ACKNOWLEDGMENT

The authors would like to thank the Director and Head – MED at Walchand College of Engineering for their assistance. This work is not supported by any funds or grants.

DECLARATION OF INTEREST STATEMENT

There are no conflicts of interest reported by the authors.

AUTHORSHIP CONTRIBUTIONS

Authors equally contributed to this work.

DATA AVAILABILITY STATEMENT

The authors confirm that the data that supports the findings of this study are available within the article. Raw data that support the finding of this study are available from the corresponding author, upon reasonable request.

CONFLICT OF INTEREST

The author declared no potential conflicts of interest with respect to the research, authorship, and/or publication of this article.

ETHICS

There are no ethical issues with the publication of this manuscript.

REFERENCES

[1] Mousavi SB, Heyhat MM. Numerical study of heat transfer enhancement from a heated circular cylinder by using nanofluid and transverse oscillation: A comparative study. J Therm Anal Calorim 2019;135:935−945. [CrossRef]

[2] Bergles AE. The implications and challenges of enhanced heat tranfer for the chemical process industries. Chem Eng Res Des 2001;79:437−444. [CrossRef]

[3] Shirazi M, Shateri A, Bayareh M. Numerical investigation of mixed convection heat transfer of a nanofluid in a circular enclosure with a rotating inner cylinder. J Therm Anal Calorim 2018;133:1061−1073. [CrossRef]

[4] Sepyani M, Shateri A, Bayareh M. Investigating the mixed convection heat transfer of a nanofluid in a square chamber with a rotating blade. J Therm Anal Calorim 2019;135:609−623. [CrossRef]

[5] Bayareh M, Amin M, Kasaeipoor A. Mixed convection heat transfer of water-alumina nanofluid in an inclined and baffled c-shaped enclosure. J Heat Mass Transf Res 2018;5:129−138.

[6] Gifford WE, Longsworth RC. Pulse-Tube Refrigeration. Trans ASME 1964;86:264−268. [CrossRef]

[7] Mikulin EI, Tarasov AA, Shkrebyonock MP. Low-Temperature Expansion Pulse Tubes. Adv Cryog Eng 1984;29:629−637. [CrossRef]

[8] Shaowei Z, Peiyi W, Zhongqi C. Double inlet pulse tube refrigerators: an important improvement. Cryogenics 1990;30:514−520. [CrossRef]

[9] Zhu SW, Zhou SL, Yoshimura N, Matsubara Y. Phase shift effect of the long neck tube for the pulse tube refrigerator. In: Ross RG, editor. Cryocoolers 9. 1st. ed. Berlin: Springer; 1997. pp. 269−278. [CrossRef]

[10] Radebaugh R. Development of the pulse tube refrigerator as an efficient and reliable cryocooler. Proc Inst Refrig 1999-2000 2000;96:11−29.

[11] Almtireen N, Brandner JJ, Korvink JG. Pulse Tube Cryocooler: Phasor Analysis and One-Dimensional Numerical Simulation. J Low Temp Phys 2020;199:1179−1197. [CrossRef]

[12] Choudhari MS, Gawali BS, Malwe P. Numerical analysis of inertance pulse tube refrigerator. IOP Conf Ser Mater Sci Eng 2021;1104:012008. [CrossRef]

[13] Hu J, Zhang L, Wang X, Zhu J, Chen S, Li H, et al. An inter-phasing stirling pulse-tube cryocooler without reservoirs. Phys Procedia 2015;67:509−512. [CrossRef]

[14] Ki T, Jeong S, Ko J, Park J. Tandem-type pulse tube refrigerator without reservoir. Cryogenics 2015;72:44−52. [CrossRef]

[15] Gao JL, Matsubara Y. An Inter-phasing pulse tube refrigerator for high refrigeration efficiency. In: Haruyama T, Mitsui T, Yamafuji K, editors. Proceedings of the Sixteenth International Cryogenic Engineering Conference/International Cryogenic Materials Conference; 1996 May 20-24; Kitakyushu, Japan: Elsevier; 1996. pp. 295−298. [CrossRef]

[16] Zhang X, Gan Z, Qiu L, Liu H. Computational fluid dynamic simulation of an inter-phasing pulse tube cooler. J Zhejiang Univ Sci A 2008;9:93−98. [CrossRef]

[17] Gour AS, Karunanithi R, Jacob S. Design of Twin Pulse Tube Cooler for 3 W @ 77 K. In: Funaki K, Nishimura A, Kamioka Y, Haruyama T, Kumakura H, editors. 24th International Cryogenic Engineering Conference and International Cryogenic Materials Conference 2012; 2012 May 14-18; Fukuoka, Japan:CERN; 2012. pp. 387−390.

[18] Gawali BS, Narayankhedkar KG. Performance prediction and experimental investigations on integral pulse tube cryocooler for 15 W at 70 K using indigenously developed linear cmpressor. AIP Conf Proc 2006;823:11−18. [CrossRef]

[19] Zhu SW, Chen ZQ. Isothermal model of pulse tube refrigerator. Cryogenics 1994;34:591−595. [CrossRef]

[20] Atrey MD, Bapat SL, Narayankhedkar KG. Cyclic simulation of Stirling cryocoolers. Cryogenics 1990;30:341−347. [CrossRef]

[21] Lin Y, Guo Z, Guo Z, Zhu S. Experimental investigation of the connecting tube effect on a step displacer type two stage pulse tube refrigerator. Appl Therm Eng 2020;173:115229. [CrossRef]

[22] Zhu S, Lin Y. Fundament of input power distribution and phase shifter functions of a step displacer type two-stage pulse tube refrigerator. Int J Refrig 2020;113:31−37. [CrossRef]

[23] Narayankhedkar KG, Gawali BS. Design and development of an orifice/inertance pulse tube cryocooler using a linear compressor. Trans Cryog Eng Conf 2004;49:1380−1387. [CrossRef]

[24] Shendage DJ, Kedare SB, Bapat SL. Numerical investigations on the Dish-Stirling engine system. Int J Ambient Energy 2019;40:274−284. [CrossRef]

[25] Shendage DJ, Kedare SB, Bapat SL. Cyclic analysis and optimization of design parameters for Beta-configuration Stirling engine using rhombic drive. Appl Therm Eng 2017;124:595−615. [CrossRef]

[26] Natu PV, Narayankhedkar KG. Cyclic analysis of the two stage stirling cycle cryogenerator. In: Haruyama T, Mitsui T, Yamafuji K, editors. Proceedings of the Sixteenth International Cryogenic Engineering Conference/International Cryogenic Materials Conference; 1996 May 20-24; Kitakyushu, Japan: Elsevier; 1996. pp. 373−376. [CrossRef]

[27] Martini W. Stirling Engine; Design Manual (NASA CR-168088). 2nd ed. Washington: US Department Energy; 1983. p. 412.

[28] ANSYS. ANSYS Fluent 12.0. Theory Guid 2009:816.

[29] Kumar P, Gupta AK, Sahoo RK, Jena DP. Numerical investigation of a 3D inertance pulse tube refrigerator from design prospective. Cryogenics 2019;98:125−138. [CrossRef]

[30] Koustubh B. Numerical simulation of 3 buffer type pulse tube cryocooler. Doctoral Thesis. Indian: National Institute of Technology Rourkela; 2018.